Hydrol. Earth Syst. Sci., 19, 3787–3805, 2015
www.hydrol-earth-syst-sci.net/19/3787/2015/
doi:10.5194/hess-19-3787-2015

Hydrology and Earth System Sciences
Open Access

Quantifying energy and water fluxes in dry dune ecosystems of the Netherlands

B. R. Voortman[1], R. P. Bartholomeus[1], S. E. A. T. M. van der Zee[2], M. F. P. Bierkens[3,4], and J. P. M. Witte[1,5]

[1]KWR Watercycle Research Institute, P.O. Box 1072, 3430 BB Nieuwegein, the Netherlands
[2]Soil Physics and Land Management, Environmental Sciences Group, Wageningen University, P.O. Box 47, 6700 AA Wageningen, the Netherlands
[3]Department of Physical Geography, Faculty of Geosciences, Utrecht University, P.O. Box 80115, 3508 TC Utrecht, the Netherlands
[4]Deltares, P.O. Box 85467, 3508 AL Utrecht, the Netherlands
[5]VU University, Institute of Ecological Science, Department of Systems Ecology, de Boelelaan 1085, 1081 HV Amsterdam, the Netherlands

Correspondence to: B. R. Voortman (bernard.voortman@kwrwater.nl)

Received: 2 April 2015 – Published in Hydrol. Earth Syst. Sci. Discuss.: 30 April 2015
Accepted: 17 August 2015 – Published: 8 September 2015

Abstract. Coastal and inland dunes provide various ecosystem services that are related to groundwater, such as drinking water production and biodiversity. To manage groundwater in a sustainable manner, knowledge of actual evapotranspiration (ET_a) for the various land covers in dunes is essential. Aiming at improving the parameterization of dune vegetation in hydrometeorological models, this study explores the magnitude of energy and water fluxes in an inland dune ecosystem in the Netherlands. Hydrometeorological measurements were used to parameterize the Penman–Monteith evapotranspiration model for four different surfaces: bare sand, moss, grass and heather. We found that the net longwave radiation (R_{nl}) was the largest energy flux for most surfaces during daytime. However, modeling this flux by a calibrated FAO-56 R_{nl} model for each surface and for hourly time steps was unsuccessful. Our R_{nl} model, with a novel submodel using solar elevation angle and air temperature to describe the diurnal pattern in radiative surface temperature, improved R_{nl} simulations considerably. Model simulations of evaporation from moss surfaces showed that the modulating effect of mosses on the water balance is species-dependent. We demonstrate that dense moss carpets (*Campylopus introflexus*) evaporate more (5 %, +14 mm) than bare sand (total of 258 mm in 2013), while more open-structured mosses (*Hypnum cupressiforme*) evaporate less (−30 %, −76 mm) than bare sand. Additionally, we found that a drought event in the summer of 2013 showed a pronounced delayed signal on lysimeter measurements of ET_a for the grass and heather surfaces, respectively. Due to the desiccation of leaves after the drought event, and their feedback on the surface resistance, the potential evapotranspiration in the year 2013 dropped by 9 % (−37 mm) and 10 % (−61 mm) for the grass and heather surfaces, respectively, which subsequently led to lowered ET_a of 8 % (−29 mm) and 7 % (−29 mm). These feedbacks are of importance for water resources, especially during a changing climate with an increasing number of drought days. Therefore, such feedbacks need to be integrated into a coupled plant physiological and hydrometeorological model to accurately simulate ET_a. In addition, our study showed that groundwater recharge in dunes can be increased considerably by promoting moss vegetation, especially of open-structured moss species.

1 Introduction

Coastal and inland sand dunes are major drinking water production sites in the Netherlands. Approximately 23 % of Dutch drinking water originates from aquifers in these dunes, which are replenished by both natural groundwater recharge and artificial infiltration of surface waters. Another ecosystem service of groundwater in dune systems is that shallow

groundwater tables sustain nature targets with a very high conservation value. Such targets, like wet dune slacks and oligotrophic pools, are often legally enforced, e.g., by the European Habitat Directive and by the Water Framework Directive. Furthermore, a deep layer of fresh groundwater in coastal dunes protects the hinterland from the inflow of saline groundwater.

Under a warming climate, summers are expected to become dryer and the water quality of surface waters may degrade (Delpla et al., 2009), especially during dry periods with low river discharge rates (Zwolsman and van Bokhoven, 2007; van Vliet and Zwolsman, 2008). To maintain current drinking water quality and production costs, water production in the future may have to rely more on natural groundwater recharge. This implies that drinking water companies need to search for new water production sites or intensify current groundwater extractions, while protecting groundwater-dependent nature targets.

For sustainable management of renewable groundwater resources, groundwater extractions should be balanced with the amount of precipitation that percolates to the saturated zone, the groundwater recharge. Knowledge of actual evapotranspiration (ET_a, here defined as the sum of plant transpiration, soil evaporation and evaporation from canopy interception) for the various land covers is essential to quantify the amount of recharge. Inland dune systems are predominantly covered with deciduous and pine forest. Well-developed hydrometeorological models are available to simulate ET_a for these forest ecosystems (Dolman, 1987; Moors, 2012). Other ecosystems, such as heathland and bare sand colonized by algae, mosses, tussock-forming grasses or lichens, received less attention. However, heathland and drift sand ecosystems have a higher conservation value than forest plantations, in particular those of coniferous trees. Nature managers are therefore often obligated to protect and develop certain heathland and drift sand ecosystems at the expense of forest ecosystems (The European Natura 2000 policy). A better parameterization of heathland and drift sand ecosystems in hydrometeorological models would aid in the sustainable management of important groundwater resources and would allow quantifying the cost and benefit of nature conservation in terms of groundwater recharge.

To this end, this study explores diurnal patterns in energy and water fluxes in a dry dune ecosystem on an elevated sandy soil in the Netherlands. Our study aims to improve the parameterization of dune vegetation in hydrometeorological models based on field measurements, focusing on four different surfaces: bare sand, moss (*Campylopus introflexus*), grass (*Agrostis vinealis*) and heather (*Calluna vulgaris*). A second objective is to quantify the effect of moss species on the water balance. Mosses and lichens are present in most successional stages in dry dune ecosystems, either as pioneer species or as understory vegetation. Voortman et al. (2014) hypothesized that moss-covered soils could evaporate less than a bare soil, since the unsaturated hydraulic properties of moss layers reduce evaporation under relatively moist conditions. Such hydraulic behavior could have large implications on the ecological interactions between vascular and nonvascular plants in water-limited ecosystems, as the presence of a moss cover could facilitate the water availability for rooting plants. Such interactions are of importance to groundwater resources, as the resilience of plant communities to drought determines the succession rate and biomass, which subsequently feedback on evapotranspiration.

A third objective is to gain insight into the delayed effect of dry spells on potential and actual evapotranspiration for heathlands and grasslands. To quantify the evapotranspiration loss term, many hydrological modeling frameworks use the concept of potential evapotranspiration ET_p (Federer et al., 1996; Kay et al., 2013; Zhou et al., 2006), defined as the maximum rate of evapotranspiration from a surface where water is not a limiting factor (Shuttleworth, 2007). ET_p is input to modeling frameworks and reduces to ET_a in cases of water stress. However, if dry spells result in a vegetation dieback, the simulated ET_p should be adjusted to account for the smaller transpiring leaf area after the dry spell. The model simulations presented in this paper give some guidance on the magnitude of errors in simulated ET_a if feedbacks of dry spells on ET_p are neglected.

The knowledge presented in this paper will help to improve and interpret the simulations of water recharge in sand dunes by hydrological models, and will sustain rainwater harvesting in dunes by vegetation management.

2 Measurements and methods

2.1 General setup

A field campaign started in August 2012 to measure energy and water fluxes in the drinking water supply area "Soestduinen", situated on an elevated sandy soil (an ice-pushed ridge) in the center of the Netherlands (52.14° latitude, 5.31° longitude). Due to deep groundwater levels, the vegetation in this region is groundwater-independent, i.e., relying solely on rainwater (on average 822 mm rain per year, 40 % falling in the first 6 months of the year and 60 % falling in the last 6 months of the year). The reference evapotranspiration according to Makkink (1957) is on average 561 mm per year. The field data were used to parameterize the Penman–Monteith equation, to calculate ET_p and to perform hydrological model simulations of ET_a, based on the actual availability of soil moisture. The Penman–Monteith equation is given by

$$ET_p = \frac{\Delta\left(R_n - G\right) + \rho_a c_p \left(e_s - e_a\right)/r_a}{\left(\Delta + \gamma\left(1 + \frac{r_s}{r_a}\right)\right)\lambda\rho_w}, \quad (1)$$

where ET_p is the potential evapotranspiration ($mm\,s^{-1}$), Δ is the slope of the saturation vapor pressure vs. temperature

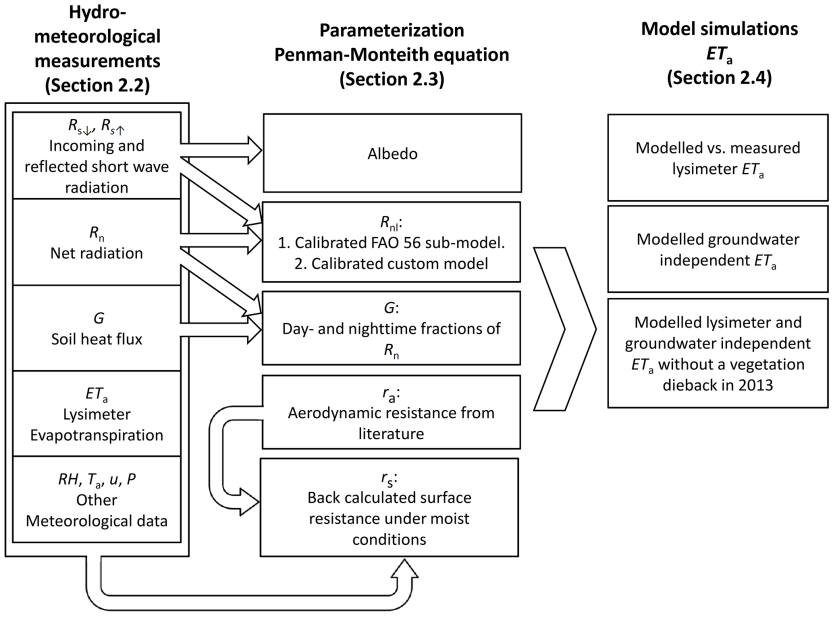

Figure 1. Organization of the research from measurements to model simulations.

curve (kPa °C^{-1}), R_n is the net radiation (J m^{-2}), G is the soil heat flux (J m^{-2}), ρ_a is the air density (kg m^{-3}), c_p is specific heat of moist air (J kg^{-1} °C^{-1}), e_s is the saturation vapor pressure of the air (kPa), e_a is the actual vapor pressure of the air (kPa), r_a is aerodynamic resistance to turbulent heat and vapor transfer (s m^{-1}), γ is the psychrometric constant (kPa °C^{-1}), λ is the latent heat of vaporization (J kg^{-1}) and ρ_w is the density of liquid water (kg m^{-3}). Results of Irmak et al. (2005) suggest that estimates of ET_p on hourly time steps are more accurate than estimates on a daily timescale. Furthermore, Liu et al. (2005) showed that the use of daily input values leads to a systematic overestimation of ET_a, especially for sandy soils. Hence, energy fluxes in the Penman–Monteith equation are preferably simulated at subdiurnal timescales. Furthermore, understanding and simulation of plant physiological processes requires knowledge of the diurnal variation of environmental variables (Nozue and Maloof, 2006). Therefore, field data were aggregated to hourly time steps to maintain the diurnal pattern and to analyze our field results at the same time interval as commonly available climate data.

In this paper evapotranspiration is defined as the sum of transpiration, soil evaporation and evaporation from canopy interception, expressed in mm per time unit. Radiative and soil heat fluxes are expressed in W m^{-2}. Figure 1 shows the procedures followed to translate field data (Sect. 2.1) to submodels of the Penman–Monteith equation (Sect. 2.2) and to subsequently calculate ET_p and simulate ET_a (Sect. 2.3).

2.2 Hydrometeorological measurements

Four homogeneous sites of bare sand, moss (*Campylopus introflexus*), grass (*Agrostis vinealis*) and heather (*Calluna vulgaris*) (Fig. 2) were selected to measure actual evapotranspiration (ET_a), the net radiation (R_n), the soil heat flux (G) and the albedo. Other meteorological variables such as wind speed (u, at 2 m above the surface), relative humidity (RH, 1.5 m above the surface), air temperature (T_a, 1.5 m above the surface) and rain (P) were measured at a weather station, installed in-between the measurement plots at a maximum distance of 40 m from each plot. Measurements were collected with data loggers (CR1000, Campbell Scientific Inc.) at a 10 s interval and aggregated to minutely values. Field measurements of bare sand, moss and grass were collected between August 2012 and November 2013. The field measurements in the heather vegetation were collected between June 2013 and November 2013.

The net radiation was measured with net radiometers (NR-Lite2 Kip & Zonen B.V.). The net radiometers were installed at a relatively low height of 32, 40, 40 and 50 cm above the bare sand, moss, grass and heather surfaces, respectively (relative to the average vegetation height), to limit the field of view to a homogenous surface. The incoming solar radiation ($R_{s\downarrow}$) and reflected solar radiation ($R_{s\uparrow}$) were measured with an albedo meter (CMA6, Kip & Zonen B.V.) that was rotated between the four surfaces. It was installed next to each R_n sensor. Due to a snow cover (winter months) or sensor maintenance (October 2012, May 2013), some periods were omitted (Fig. 3).

Eight self-calibrating heat flux plates (HFP01SC, Hukseflux B.V.) (two for each site) were installed 8 cm below the

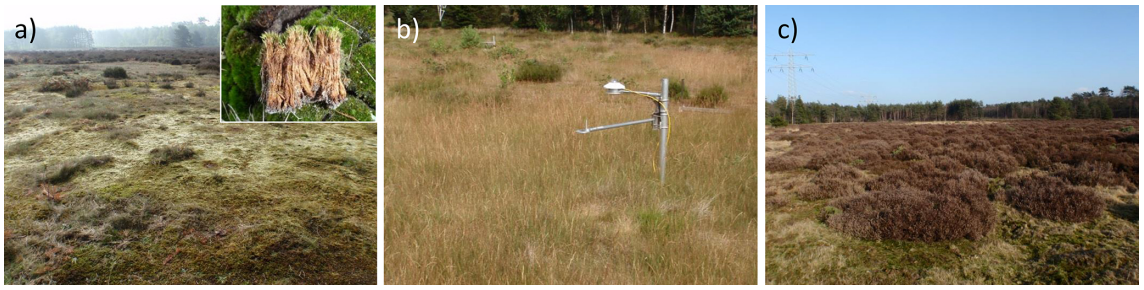

Figure 2. The vegetation types studied in this paper, **(a)** the moss surface with an approximately 2 cm thick layer of *Campylopus introflexus* (inset), **(b)** the grass surface, primarily *Agrostis vinealis* and **(c)** the heather surface, *Calluna vulgaris*.

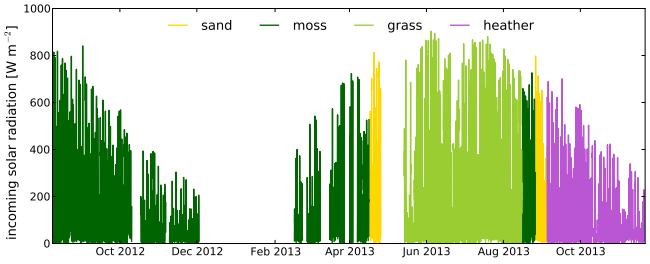

Figure 3. Measured incoming solar radiation $R_{s\downarrow}$ at the four different surfaces. Periods with snow cover or sensor maintenance were omitted.

soil surface near the net radiometers. These heat flux plates were programmed to calibrate themselves for 15 min at 6 h time intervals, based on a known heat flux supplied by an integrated heater. Besides each soil heat flux plate, an averaging thermocouple (TCAV, Campbell Scientific, Inc.) was installed at 2 and 6 cm depth and a soil moisture probe (CS616, Campbell Scientific, Inc) was installed at 4 cm depth to estimate the change in heat storage (S) above the heat flux plates. The sum of the measured soil heat flux at 8 cm depth and S represents the heat flux at the soil surface. Sensor installation and procedures to calculate S were followed according to the Campbell Scientific Inc. (2014) HFP01SC instruction manual.

Within each surface, one weighing lysimeter was installed. The lysimeters (Fig. 4) had a 47.5 cm inner diameter and were 50 cm deep. Intact soil monoliths were sampled by hammering the PVC tube into the soil, alternated with excavating the surrounding soil to offset soil pressures. The lysimeters were turned upside down, to level the soil underneath and to close this surface with a PVC end cap. To allow water to drain out of the lysimeter bottom plate, a 2.5 cm diameter hole was made in the base plate. A 15 cm long fiberglass wick (Pepperell $2 \times 1/2$ inch) was installed in the PVC end cap to guide drainage water through the hole into a tipping bucket (Davis 7852) below the lysimeter. The wick, together with two sheets of filter cloth (140–150 µm, Eijkelkamp Agrisearch Equipment), placed at the bottom of the lysimeter tank, prevented soil particles from flushing out

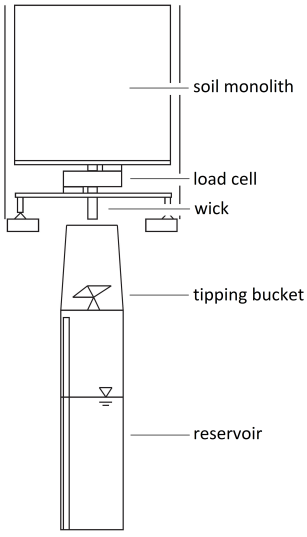

Figure 4. Lysimeter design.

of the lysimeter. The tipping bucket below the lysimeter had a resolution of 0.2 mm for the intercepting area of the tipping bucket, which was equal to 0.024 mm for the cross-sectional area of the lysimeter. Drainage water was collected in a reservoir installed below the lysimeter.

The lysimeters were weighted with temperature compensated single point load cells (Utilcell 190i, max 200 kg). These load cells were initially connected to the full bridge data ports of the data loggers. However, the measurement resolution of the data loggers was too coarse to fully compensate for temperature effects on weight measurements. Fluctuations of 0.333 µV due to temperature effects were within the data logger measurement resolution, which equals 36 g in weight change, i.e., 0.2 mm of evaporation. To increase the lysimeter precision, digitizers (Flintec LDU 68.1) were installed in May 2013 to process and digitize the load cell signals without interference of the data logger. In this setup, a measurement resolution of 10 g was achieved, i.e., 0.06 mm equivalent water depth, which is adequate for measuring ET_a for daily time periods (subtracting two values would lead to a maximum error of 0.06 mm caused by the measurement res-

olution). Analysis of measured ET_a was therefore limited to the period after installation of the digitizers.

After a rain event on 7 September 2013, the tipping buckets below the grass and heather lysimeters became partly clogged with beetles nesting underneath the lysimeters. This led to a continuous drainage signal which was out of phase with the weight measurements. Without accurate drainage measurements, lysimeter weight signals cannot be transferred to evapotranspiration. Therefore, ET_a data on days with a poor drainage signal after 7 September 2013 were disregarded in the analyses for the grass and heather lysimeters.

2.3 Parameterization of the Penman–Monteith equation

2.3.1 Net radiation (R_n)

The net radiation (R_n) is defined as

$$R_n = R_{ns} + R_{nl} = (1 - \text{albedo})\, R_{s\downarrow} + \left(\varepsilon_s R_{l\downarrow} - R_{l\uparrow}\right), \quad (2)$$

where R_{ns} is the net shortwave radiation, R_{nl} is the net longwave radiation, $R_{s\downarrow}$ is the incoming solar radiation, $R_{l\downarrow}$ is the downwelling longwave radiation from the atmosphere to the surface, $R_{l\uparrow}$ is the emitted longwave radiation by the surface into the atmosphere and ε_s is the surface emissivity representing the reflected downwelling longwave radiation. The albedo in Eq. (2) was determined by linear regression between measured $R_{s\downarrow}$ and $R_{s\uparrow}$. Based on the albedo obtained this way, R_{nl} follows from measurements of R_n by subtracting calculated R_{ns} from measured R_n. Throughout this paper, this back-calculated R_{nl} is referred to as the measured R_{nl}.

In hydrometeorological models, R_{nl} is commonly estimated under clear sky conditions and multiplied by a factor to correct for clouds (Irmak et al., 2010; Gubler et al., 2012; Blonquist Jr. et al., 2010; Temesgen et al., 2007). A similar approach was followed in this study in which the Stefan–Boltzmann law is substituted into Eq. (2) for $R_{l\downarrow}$ and $R_{l\uparrow}$ under clear sky conditions (Saito and Šimůnek, 2009; Van Bavel and Hillel, 1976) and multiplied by a cloudiness function to obtain R_{nl}:

$$R_{nl} = \left(\varepsilon_s \varepsilon_a \sigma T_a^4 - \varepsilon_s \sigma T_s^4\right) f_{cd}, \quad (3)$$

where ε_a is the clear sky emissivity of the atmosphere (–), ε_s is the surface emissivity (–), σ is the Stefan–Boltzmann constant ($5.67 \times 10^{-8}\,\mathrm{W\,m^{-2}\,K^{-1}}$), T_a is the air temperature (K), T_s is the surface temperature (K) and f_{cd} is a cloudiness function (–; described later). For vegetated surfaces, $\varepsilon_s = 0.95$ was used (based on Jones, 2004), and $\varepsilon_s = 0.925$ was used for bare sand (based on Fuchs and Tanner, 1968). Estimating ε_a has a long history and numerous parameterizations are available. In this study, the empirical relationship found by Brunt (1932) was used:

$$\varepsilon_a = 0.52 + 0.065\sqrt{e_a}, \quad (4)$$

where e_a is the water vapor pressure measured at screen level (hPa). The cloudiness function f_{cd} in Eq. (3) is limited to $0.05 \le f_{cd} \le 1$ and equal to

$$f_{cd} = \frac{R_{s\downarrow}}{R_{s0}}, \quad (5)$$

where R_{s0} is the estimated clear sky solar radiation. We estimated R_{s0} following the FAO irrigation and drainage paper No. 56 (Allen et al., 1998). Since f_{cd} is undefined during the night, an interpolation of f_{cd} between sunset and sunrise is required. According to Gubler et al. (2012) f_{cd} can be best linearly interpolated between the 4 to 6 h average before sunset and after sunrise. We adopted this approach, applying a 5 h average.

An estimate of T_s is required to fully parameterize Eq. (3). We developed a new approach to simulate the diurnal pattern in T_s. Using Eq. (3), we back-calculated $T_s - T_a$ based on measured R_{nl} for clear hours ($f_{cd} > 0.9$). Generally, $T_s - T_a$ will be negative during nighttime (when solar elevation β (radians) < 0), and will gradually increase to positive values during daytime ($\beta > 0$ 0). We describe this pattern by (Fig. 5):

$$T_s - T_a = f_{cum}\left(\beta, \mu_\beta, \sigma_\beta\right)\left(T_{s,\,amp} + \beta T_{s,\,slope}\right) + T_{s,\,offset}, \quad (6)$$

where f_{cum} is a cumulative normal distribution function with mean μ_β and standard deviation σ_β, describing the moment at which the surface becomes warmer than the air temperature (μ_β) and the speed at which the surface warms up or cools down (σ_β) as a function of solar elevation angle (β). $T_{s,amp}$ is the amplitude of T_s (K), $T_{s,slope}$ is the slope between β and $T_s - T_a$ during daytime ($\mathrm{K\,radians^{-1}}$) and $T_{s,offset}$ is the average value of $T_s - T_a$ during nighttime (K). The parameters of Eq. (6), except $T_{s,offset}$, were fitted to the data by minimizing the root mean square error (RMSE) by generalized reduced gradient nonlinear optimization. The $T_{s,offset}$ was determined as the average nighttime $T_s - T_a$ to limit the number of parameters during the optimization. Equation (6) was substituted for T_s in Eq. (3) to estimate R_{nl}. This novel approach to derive R_{nl} was compared to the R_{nl} model of the FAO-56 approach (Allen et al., 1998), originally derived to obtain daily estimates of R_{nl} (using minimum and maximum daily T_a divided by 2 instead of T_a in Eq. 7) but commonly applied at hourly timescales (ASCE-EWRI, 2005; Perera et al., 2015; Gavilán et al., 2008; López-Urrea et al., 2006):

$$R_{nl} = -\sigma T_a^4 \left(a - b\sqrt{e_a}\right)\left(1.35\frac{R_s}{R_{s0}} - 0.35\right), \quad (7)$$

where the first term between brackets represents the net emittance, which should compensate for the fact that T_s is not measured. The empirical parameters a and b can be calibrated for a specific climate and/or vegetation. The second term between brackets is a cloudiness function. The default

parameter values for a and b are 0.34 and 0.14, respectively (Allen et al., 1998). We calibrated these parameters for every site by linear least squares regression for clear days ($R_s/R_{s0} > 0.9$) and compared the performance of both R_{nl} models (Eqs. 3, 7).

2.3.2 Soil heat flux (G)

The soil heat flux is commonly expressed as a fraction of R_n, particularly on large scales using remote sensing (Su, 2002; Bastiaanssen et al., 1998; Kustas et al., 1998; Kustas and Daughtry, 1990; Friedl, 1996). We adopted the same approach, making a distinction between daytime (F_{day}) and nighttime (F_{night}) fractions, determined by linear least squares regression between R_n and the average of the two sets of soil heat flux measurements.

2.3.3 Aerodynamic resistance (r_a)

The aerodynamic resistance under neutral stability conditions can be estimated by (Monteith and Unsworth, 1990)

$$r_a = \frac{\ln\left[\frac{z_m - d}{z_{om}}\right] \ln\left[\frac{z_h - d}{z_{oh}}\right]}{k^2 u_z}, \quad (8)$$

where z_m is the height of wind speed measurements (m), d is the zero plane displacement height (m), z_{om} is the roughness length governing momentum transfer (m), z_h is the height of the humidity measurements (m), z_{oh} is the roughness length governing transfer of heat and vapor (m), k is the von Karman's constant (0.41 (–)) and u_z is the wind speed at height z_m ($m\,s^{-1}$). For grass, empirical equations are developed (FAO-56 approach) to estimate d, z_{om} and z_{oh}:

$$d = 0.66V \quad (9)$$

$$z_{om} = 0.123V \quad (10)$$

$$z_{oh} = 0.1 z_{om}, \quad (11)$$

where V is the vegetation height. Wallace et al. (1984) found comparable coefficients for heather: $d = 0.63V$ and $z_{om} = 0.13V$ and therefore Eqs. (9)–(11) were applied for both surfaces using a constant vegetation height of 7 and 31 cm for the grass and heather surfaces, respectively. For the moss surface, we used a vegetation height of 2 cm, which is equal to the thickness of the moss mat. For the bare sand surface we assumed $d = 0$ m, and used typical surface roughness values published by Oke (1978): $z_{oh} = 0.001$ m and $z_{om} = z_{oh}$.

2.3.4 Surface resistance (r_s) and canopy interception

Canopy interception was simulated as a water storage which needs to be filled before rainwater reaches the soil surface. A maximum storage capacity of 0.50 mm was defined for heather following the study of Ladekarl et al. (2005). To our knowledge no literature value of the interception capacity of the specific grass species (*Agrostis vinealis*) is published. Considering the relatively low vegetation height, we assumed a maximum interception capacity of 0.25 mm.

We distinguished wet (r_{swet}) and dry canopy surface resistance (r_s), since interception water evaporates without the interference of leaf stomata. During canopy interception (i.e., if the interception store is fully or partly filled), we used a surface resistance of $0\,s\,m^{-1}$, reducing Eq. (1) to the Penman equation (Penman, 1948; Monteith and Unsworth, 1990). After the canopy storage is emptied, the surface resistance switches to r_s. The r_s was back-calculated for daytime periods for the heather and grass lysimeters by substituting measured R_n, G, ET_a, e_s and e_a and simulated r_a into Eq. (1) under nonstressed conditions (i.e., $ET_p = ET_a$). Nighttime evaporation was assumed to be equal to 0 mm. To make sure that the back-calculated r_s was based on days at which evapotranspiration occurred at a potential rate, it was back-calculated for every two consecutive days after precipitation events and after emptying of the (calculated) interception store. The surface resistance (r_s) of bare sand and moss was assumed to be equal to $10\,s\,m^{-1}$, i.e., similar to the surface resistance under well-watered conditions of bare soil found by Van de Griend and Owe (1994).

During the summer of 2013, a dry spell (from 4 until 25 July 2013) resulted in a vegetation dieback of grass and heather. Surface resistances were back-calculated for periods before and after the drought event. The drought event had 22 consecutive dry days with a cumulative reference evapotranspiration of 85 mm according to Makkink (1957). Drought events of similar magnitude have been recorded 12 times during the past 57 years (from 1958 until 2014) at climate station "de Bilt" located in the center of the Netherlands (52.1° latitude, 5.18° longitude), 10 km from the measurement site. The measurements in the heather vegetation started a week before the drought event. During this week, there were 2 days (30 June and 1 July 2013) for which r_s could be back-calculated. The estimated r_s for these days was 35 and $107\,s\,m^{-1}$ respectively. We selected the r_s value of the second day to use in our model simulations ($107\,s\,m^{-1}$) because it was in close agreement with the median surface resistance found by Miranda et al. (1984) of $110\,s\,m^{-1}$ in a comparable heather vegetation. After the drought event, r_s increased to $331\,s\,m^{-1}$ ($N = 14$, standard error $= 102\,s\,m^{-1}$). For the grass vegetation, the surface resistance before the drought event was $181\,s\,m^{-1}$ ($N = 9$, standard error $= 68\,s\,m^{-1}$). After the drought event, the surface resistance increased to $351\,s\,m^{-1}$ ($N = 4$, standard error $= 47\,s\,m^{-1}$). Since mosses of these habitats are desiccation-tolerant and quickly rehydrate after drought (Proctor et al., 2007), we did not assess the effect of the dry spell on the surface resistance of the moss surface.

The parameters thus obtained were used to parameterize the Penman–Monteith equation and to calculate hourly ET_p values for each surface.

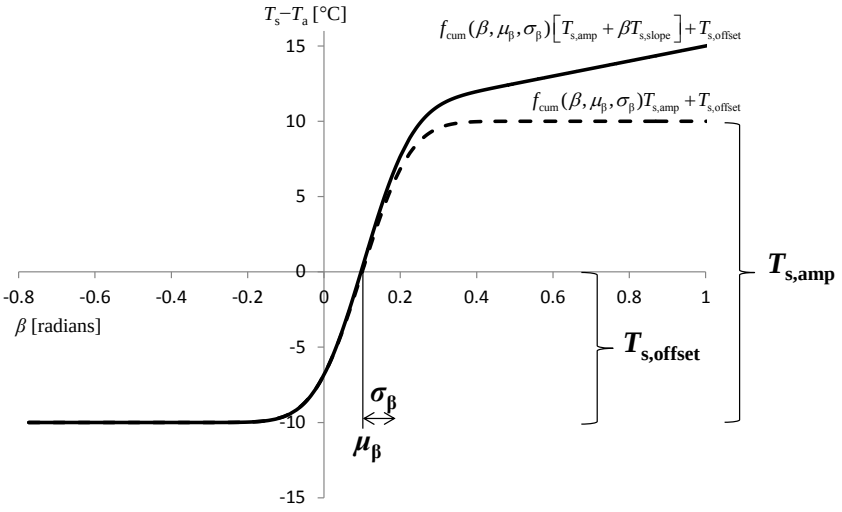

Figure 5. Equation (6) and associated parameters to describe the surface–air temperature difference, substituted for T_s in R_{nl} (Eq. 3).

2.4 Model simulations of ET_a

Using hourly ET_p for the year 2013 (876 mm precipitation), we used Hydrus 1D (Šimůnek et al., 2008) to simulate ET_a. If meteorological data of the local weather station were missing due to snow cover or sensor maintenance, the meteorological data of weather station "de Bilt" were used for the calculation of ET_p.

First, we simulated ET_a for the lysimeter surfaces and compared our results with the lysimeter measurements of ET_a. The lower boundary condition in the model was a seepage face with hydraulic pressure equal to 0 at a depth of 65 cm below the surface (50 cm soil and 15 cm wick). This boundary condition assumes that the boundary flux will remain zero as long as the pressure head is negative. When the lower end of the soil profile becomes saturated, a zero pressure head is imposed at the lower boundary and outflow calculated accordingly. Second, we simulated ET_a for the groundwater-independent surroundings. We expected that the availability of soil moisture in the lysimeter tanks to be larger than in the groundwater-independent surroundings, because the lowest sections of the lysimeters need to be saturated before drainage occurs. To estimate the yearly ET_a of dune vegetation in environments with deep groundwater levels, we used a free drainage boundary condition (i.e., a pressure head gradient of 0 and an elevation head of 1) located 2.5 m below the surface. Third, we investigated the magnitude of the vegetation dieback in the summer of 2013 on both ET_p and ET_a, by using two different surface resistances: one derived from the period before, and one for the period after the vegetation dieback.

Soil hydraulic properties in the hydrological model were described by the Van Genuchten relationships (Van Genuchten, 1980). Soil samples (100 cm^3) collected next to each lysimeter at 5 and 15 cm depth were used to derive the drying retention function. The average drying retention parameters (of the two samples collected next to each lysimeter) were used in the hydrological model, taking hysteresis into account by assuming the wetting retention curve parameter (α_{wet}) to be twice as large as the drying retention curve parameter (α_{dry}) (Šimůnek et al., 1999). The unsaturated hydraulic properties (parameters l and K_0) were estimated using the Rosetta database and pedotransfer functions, providing the fitted drying retention curve parameters as input (Schaap et al., 2001). The hydraulic properties of the 15 cm long wick, guiding drainage water below the lysimeter into the tipping bucket, were taken from Knutson and Selker (1994).

Since mosses have neither leaf stomata nor roots, ET_a from the moss surface is limited by the capacity of the moss material to conduct water to the surface. This passive evaporation process is similar to the process of soil evaporation, i.e., evaporation becomes limited if the surface becomes too dry to deliver the potential rate. The unsaturated hydraulic properties of the dense *Campylopus introflexes* moss mat covering the lysimeter soil were based on the hydraulic properties derived by Voortman et al. (2014) and used in the first 2 cm of the model domain. Macro pores in the moss mat were neglected by Voortman et al. (2014), which implies that direct implementation of these hydraulic properties would result in large amounts of surface runoff generation or ponding, since the unsaturated hydraulic conductivity (K_0) of the moss mat is lower than 0.28 cm d^{-1}. Therefore, the dual porosity model of Durner (1994) was used to add 1000 cm d^{-1} to the hydraulic conductivity curve of Voortman et al. (2014) between -1 and 0 cm pressure head (Appendix A). This permits the infiltration of rainwater at high intensity rain showers without affecting the unsaturated hydraulic behavior at negative pressure heads. Because of the complex shape of the retention function of the moss mat, hysteresis in the soil

hydraulic functions in the underlying soil was neglected for the simulation of evaporation from moss surfaces. The sensitivity of this simplification on the model outcomes was investigated by adjusting the soil hydraulic function of the soil from the drying to the wetting curve. This had a negligible effect (< 1 mm) on the simulated yearly ET_a (data not shown). Besides simulations of moss evaporation with a cover of *Campylopus introflexus*, soil physical characteristics of *Hypnum cupressiforme* were used in the first 2 cm of the model domain to analyze the effect of different moss species on the water balance. Soil parameters used in the model are explained in more detail in Appendix A.

Since the grass and heather lysimeters fully covered the soil, soil evaporation was neglected for these surfaces. The root profile for the grass and heather lysimeters was 30 cm deep, with the highest concentration of roots in the upper layer decreasing linearly with depth. A water stress reduction function (Feddes et al., 1978) was used to simulate the closure of leaf stomata during water-stressed periods. Vegetation parameters are explained in more detail in Appendix B. Modeled actual evapotranspiration ($ET_{a,mod}$) was aggregated to daily values and compared to field measurements of ET_a during moist ($ET_{a,mod} = ET_p$) and dry conditions ($ET_{a,mod} \neq ET_p$).

2.5 Model performance assessment

Model performance of R_{ns}, R_{nl}, G and $ET_{a,mod}$ simulations were tested with the Nash–Sutcliffe model efficiency coefficient (NSE):

$$\mathrm{NSE} = 1 - \frac{\sum_{t=1}^{N}\left(x_{o,t} - x_{m,t}\right)^2}{\sum_{t=1}^{N}\left(x_{o,t} - \bar{x}_o\right)^2}. \quad (12)$$

where N is the total number of observations, $x_{m,t}$ is the model-simulated value at time step t, $x_{o,t}$ is the observed value at time step t, and $\bar{x}$ is the mean of the observations. NSE $= 1$ corresponds to a perfect match of modeled to observed data. If NSE < 0, the observed mean is a better predictor than the model. To assess the magnitude of error of model simulations, the root mean square error (RMSE), the mean difference (MD) and the mean percentage difference (M%D) were used.

3 Results and discussion

3.1 Parameterization of the Penman–Monteith equation

3.1.1 Net shortwave radiation

The measured incoming and reflected solar radiation were used to compute the albedo of the four surfaces by linear regression (Fig. 6; Table 5). This single value for the albedo slightly overestimates the reflected solar radiation at large incoming solar radiation (Fig. 7) because of a dependency of the albedo on solar elevation angle β (Yang et al., 2008; Zhang et al., 2013). Nonetheless the use of a single value for the albedo hardly affects the error in modeled R_{ns}; the mean difference (MD) between measured and modeled R_{ns} lies between -0.23 and $1.63\,\mathrm{W\,m^{-2}}$ (Table 1), which is equal to the energy required to evaporate 0.008 to $0.057\,\mathrm{mm\,d^{-1}}$. The NSE for estimating R_{ns} is close to 1 (Table 1), showing almost a perfect match of modeled to observed data.

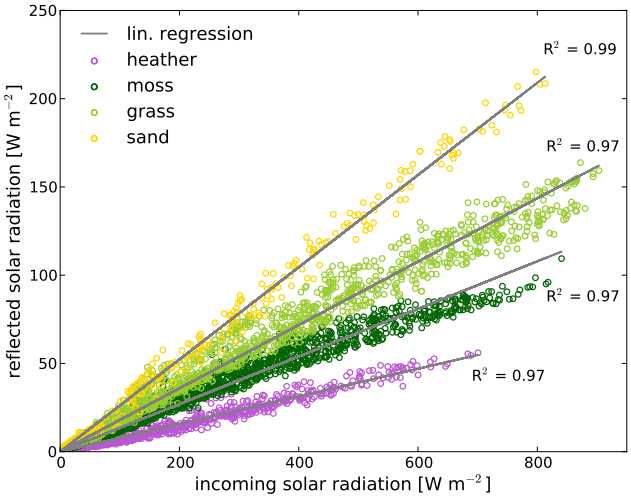

Figure 6. Linear regression between incoming and reflected solar radiation.

The dense moss mat *Campylopus introflexes* entirely covers the underlying mineral soil, which results in a low albedo (0.135) due to the dark green surface. The albedo of bare sand (0.261) is comparable to values found in literature for bare dry coarse soils (Qiu et al., 1998; Van Bavel and Hillel, 1976; Linacre, 1969; Liakatas et al., 1986) and the albedo for grass (0.179) is consistent with values reported in other studies during summer time (Hollinger et al., 2010) or for dried grass (Van Wijk and Scholte Ubing, 1963). Heather has a somewhat lower albedo (0.078) than was found in the literature: Miranda et al. (1984) report an albedo of 0.13 (*Calluna*, LAI ca. 4); Wouters et al. (1980) report an albedo of 0.102 (*Calluna*). The heather vegetation in our study was in a later successional stage with aging shrubs having a relatively large fraction of twigs and a smaller LAI (3.47) than found by Miranda et al. (1984). Furthermore, the albedo data of heather vegetation were collected primarily past the growing season from September till November. The darker surface after the growing season and the lower LAI explains the small albedo compared to other studies.

3.1.2 Net longwave radiation

The fitted function of Eq. (6) describes the dynamics of the surface temperature relative to air temperature (Fig. 8, Table 5). All surfaces have a similar average nighttime surface

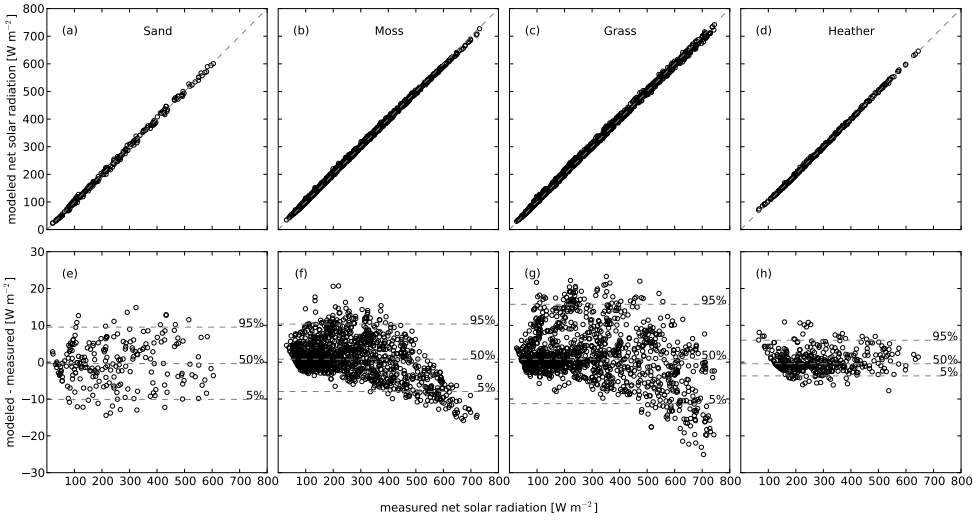

Figure 7. Modeled compared to measured net solar radiation (panels **a–d**, dashed lines are 1 : 1 lines) and deviations from the 1 : 1 line (panels **e–h**; dashed lines indicate 5, 50 and 95 percentiles).

Table 1. Model performance of R_{ns} simulations.

Surface	N	NSE	RMSE ($W m^{-2}$)	MD ($W m^{-2}$)	M%D (%)
Sand	218	0.998	5.99	−0.23	−0.10
Moss	1317	0.999	5.46	1.18	0.46
Grass	1203	0.998	7.78	1.63	0.55
Heather	407	0.999	3.00	0.24	0.09

temperature ($T_{s,offset}$) relative to T_a, ranging between −7.47 and −10.21 °C. The solar elevation angle at which the surfaces become warmer than the air temperature (μ_β), as well as the speed at which the surface warms up or cools down (σ_β), are comparable between the surfaces. The main difference between the surfaces is observed at high solar elevation angles. Sand and moss show a clear increasing slope during the day, while grass and heather are able to attenuate the increase in surface temperature, possibly due to a larger latent heat flux (Fig. 8). The moss surface shows the largest increase in surface temperature during the day. Although organic layers, e.g., dry peat, have a larger specific heat (1600 $J kg^{-1} K^{-1}$) than dry sand (693 $J kg^{-1} K^{-1}$) (Gavriliev, 2004), the energy required to heat up the moss material is much smaller than for sand, because of the small dry bulk density of ca. 26.8 $g L^{-1}$ (derived for *Campylopus introflexus* from Voortman et al., 2014). Therefore, the surface temperature and the emitted longwave radiation are largest for the moss surface.

Our R_{nl} model (Eqs. 3 and 6) simulates R_{nl} much better than the calibrated (Table 2) FAO-56 R_{nl} submodel (Table 3). For the natural grass surface, the NSE even becomes negative using the calibrated FAO-56 approach. Several studies

Table 2. Calibrated net emissivity parameters of the FAO-56 R_{nl} submodel (Eq. 7).

	a	b
Sand	0.31	−0.00
Moss	0.33	0.02
Grass	0.36	−0.06
Heather	0.24	0.02

Table 3. Model performance of R_{nl} simulations for hourly time steps.

Surface	N	NSE	RMSE ($W m^{-2}$)	MD ($W m^{-2}$)	M%D (%)
Using Eq. (3)					
Sand	5891	0.65	27.37	0.92	1.52
Moss	5997	0.74	28.57	3.73	5.19
Grass	6113	0.71	25.66	1.41	2.36
Heather	2424	0.63	27.63	−0.21	−0.40
Using FAO-56 Eq. (7)					
Sand	5891	0.41	35.39	4.34	7.14
Moss	5997	0.31	46.67	14.84	20.65
Grass	6113	−0.07	49.41	−18.23	−30.38
Heather	2424	0.29	38.24	10.50	19.54

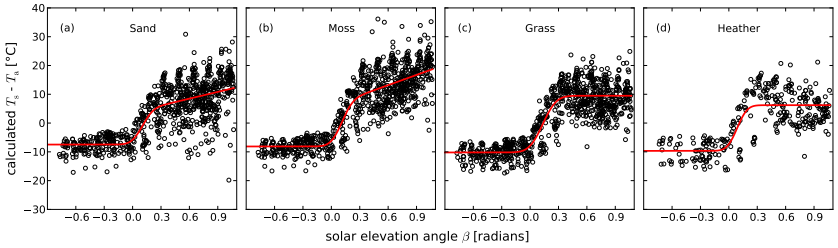

Figure 8. Measured surface temperature relative to air temperature (T_s–T_a) for clear hours ($f_{cd} > 0.9$) as a function of solar elevation angle β. Relationships (red lines) were fitted to the data using Eq. (6).

showed that the FAO-56 R_{nl} submodel underestimates the magnitude of R_{nl} for reference grass vegetation and poorly describes the diurnal pattern (Matsui, 2010; Blonquist Jr. et al., 2010; Yin et al., 2008; Temesgen et al., 2007). As mentioned, the FAO-56 R_{nl} submodel was originally developed for reference grass vegetation under well-watered conditions for daily time steps, but is commonly applied at hourly timescales (ASCE-EWRI, 2005; Perera et al., 2015; Gavilán et al., 2008; López-Urrea et al., 2006; Irmak et al., 2005). At daily time steps, T_s is close to T_a, since the warmer daytime T_s is compensated by the cooler nighttime T_s. For hourly time steps, the assumption that T_s follows T_a is not valid, which explains the poor performance of the FAO-56 R_{nl} model for hourly time steps. This poor performance cannot be compensated by calibrating the net emissivity parameters, since the diurnal pattern remains unaffected.

In this analysis a typical pattern in T_s relative to T_a is used to estimate T_s (Eq. 6), and subsequently R_{nl} (Eq. 3). This relationship (Fig. 8) is sensitive to local weather conditions, which implies that the parameters of Eq. (6) (Table 5) are not directly transferable to other locations or climates. The applicability of the presented approach to simulate R_{nl} should be tested before it is used for other surfaces or climates. It should be noted that the number of parameters that are required to simulate R_{nl} is relatively large. However, μ_β as well as σ_β, are comparable between the surfaces. These parameters might be assumed similar for every surface, reducing the species-specific model parameters to three (one more than the FAO-56 approach). More data of different vegetation types are required to generalize these results and to assess the number of parameters that are required to accurately simulate R_{nl}.

3.1.3 Soil heat flux

The soil heat flux G as a fraction of R_n (F_{day} and F_{night}) decreases with vegetation cover (Table 5). The nighttime fractions are larger than the daytime fractions, as R_n becomes smaller in magnitude during the night, which simultaneously corresponds to a change in direction of R_n and G, from downward (positive) to upward (negative). Relatively small systematic errors are made using daytime and nighttime fractions of R_n to simulate G (MD between 1.92 and 0.69 W m^{-2}) (Table 4). In remote sensing algorithms G is often simulated as fraction of R_n, depending on the LAI or the fractional vegetation cover. In e.g., the SEBS algorithm, the soil heat flux fraction (F) is interpolated between 0.35 for bare soil and 0.05 for a full vegetation canopy (Su, 2002). These limits are close to the bare sand (0.270) and heather (0.066) F_{day} fractions (Table 5). The heather F_{day} (0.066) was close to the value found by Miranda et al. (1984) of 0.04.

The analysis of the relationship between R_n and G was based on the average of two sets of soil heat flux plates per surface. These sets of measurements showed on average a good agreement: a MD below 1.07 W m^{-2}, with a RMSE ranging between 5.02 and 9.40 W m^{-2}.

Table 4. Model performance of G simulations.

Surface	N	NSE	RMSE (W m^{-2})	MD (W m^{-2})	M%D (%)
Sand	6080	0.820	20.06	1.92	22.16
Moss	5335	0.901	12.02	1.65	24.29
Grass	6046	0.868	8.97	1.60	43.42
Heather	2028	0.641	11.39	0.69	40.27

Table 5. Parameters of the four different surfaces used for the calculation of ET_p for hourly time steps.

Parameter	Sand	Moss	Grass	Heather
Albedo (–)	0.261	0.135	0.179	0.078
μ_β (radians)	0.10	0.10	0.13	0.09
σ_β (radians)	0.09	0.09	0.11	0.08
$T_{s,amp}$ (°C)	11.26	14.21	19.70	15.89
$T_{s,offset}$ (°C)	−7.47	−8.14	−10.21	−9.67
$T_{s,slope}$ (°C radians^{-1})	7.83	11.82	0.00	0.00
F_{day} (–)	0.270	0.211	0.129	0.066
F_{night} (–)	0.761	0.647	0.527	0.462
r_{swet} (s m^{-1})	–	–	0	0
r_s (s m^{-1}) before drought	10	10	181	107
r_s (s m^{-1}) after drought	10	10	351	331

3.1.4 Energy balance

All the terms in the energy balance can be defined using daily lysimeter measurements of LE (latent heat flux) and an estimate of the sensible heat flux (H) as a residual term of the energy balance. For daytime measurements (between sunrise and sunset), the LE, H, G, $R_{s\uparrow}$ and R_{nl} can be expressed as fraction of the $R_{s\downarrow}$. Table 6 summarizes the average fraction of $R_{s\downarrow}$ attributed to these five different energy fluxes during the measurement campaign. The net longwave radiation is for most surfaces the largest energy flux during daytime (Table 6).

The LE of most surfaces is the second largest flux during daytime, of which fraction increases with vegetation cover. Despite the large difference in albedo between bare sand and moss, the moss surface has only a slightly larger LE fraction than bare sand (Table 6). This is primarily caused by the larger R_{nl} flux of moss, which compensates the smaller amount of reflected solar radiation.

Table 6. Average fractionation of the incoming shortwave radiation ($R_{s\downarrow}$) between different energy fluxes during daytime.

Surface	LE	H	G	$R_{s\uparrow}$	R_{nl}
Sand	0.22	0.13	0.10	0.26	0.28
Moss	0.24	0.17	0.09	0.14	0.36
Grass	0.27	0.21	0.06	0.18	0.29
Heather	0.35	0.20	0.05	0.08	0.32

3.2 Potential and actual evapotranspiration

The modeled ET_a is in agreement with the measured ET_a, with some exceptions at the onset of dry out events (Fig. 9). In general, the reduction of ET_p to ET_a is modeled a few days later than it emerges from measurements. The cumulative $ET_{a,mod}$ over the measurement period (May–October 2013) deviates 21 mm (13 %), −13 mm (−7 %), 5 mm (2 %) and −3 mm (−2 %) from the measured ET_a of the sand, moss, grass and heather lysimeters, respectively. The results of modeled vs. measured ET_a for non-water-stressed ($ET_a = ET_p$) and water-stressed conditions ($ET_{a,mod} < ET_p$) are summarized in Table 7.

We did not calibrate our model, e.g., by adjusting soil hydraulic properties, because several processes outlined by Allen et al. (1991) and wall flow (Cameron et al., 1992; Corwin, 2000; Till and McCabe, 1976; Saffigna et al., 1977) affect lysimeter measurements of ET_a and drainage. We suspect that wall flow caused the slightly earlier reduction of ET_p to ET_a at the onset of dry out events than was simulated by the model. Wall flow leads to a quicker exfiltration of rainwater and a subsequent lower moisture content in the lysimeter, and therefore a slightly earlier timing of drought compared to the model. Since wall flow does not occur in the undisturbed vegetation outside the lysimeters, calibrating e.g., soil hydraulic properties using measured surface and drainage fluxes in the objective function could lead to biased characterizations of the soil hydraulic properties and erroneous simulations of soil water flow and ET_a.

In our simulations, we neglected vapor flow within the soil and moss layer. Due to temperature and potential gradients, vapor fluxes may occur through the soil and moss layer in upward and downward direction by diffusion. Vapor flow may occur by advection as well, e.g., through macropores. Water and vapor flows act together and are hard to distinguish.

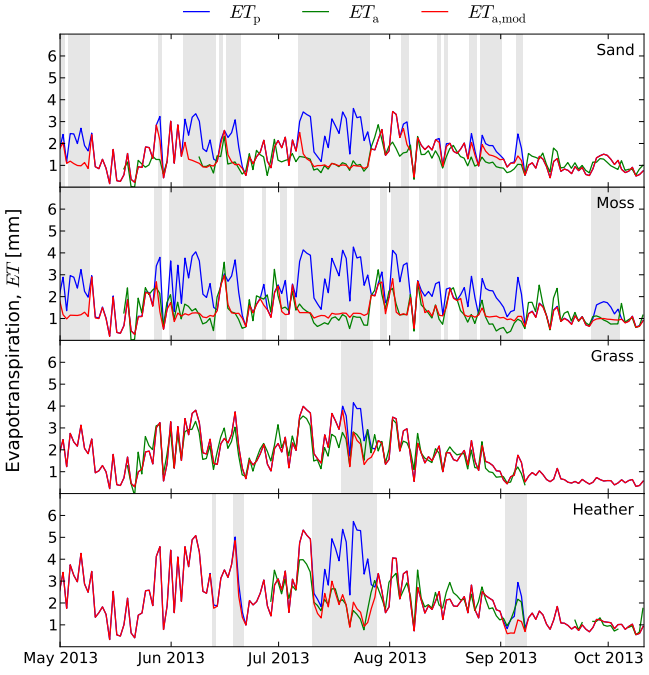

Figure 9. Measured and modeled daily ET for the four lysimeters. Gray bars indicate time periods where $ET_{a,mod}$ is smaller than ET_p, i.e., when evapotranspiration was water-limited.

Modeling and lab experiments show a minor cumulative effect of vapor flow on evaporation for moist and temperate climates. Soil evaporation in a temperate climate for loamy sand in Denmark was only slightly smaller (1.5 %) than a simulation excluding vapor flow (Schelde et al., 1998). Experiments of Price et al. (2009) show that only 1 % of the total water flux was caused by vapor flow in columns of *Sphagnum* moss. Nevertheless, for a dry and warm Mediterranean climate – different from ours – Boulet et al. (1997) found a dominant vapor flux down to a depth of 25 cm in a bare soil during 11 days in a dry and warm Mediterranean climate. Because large temperature and potential gradients occur when $ET_a \neq ET_p$, vapor flow could especially become dominant in the water-limited phase of evaporation. We compared the model performance between dry ($ET_{a,mod} \neq ET_p$) and wet ($ET_{a,mod} = ET_p$) days in Fig. 10. The model performance in both moisture conditions is comparable (RMSE of sand when dry was 0.40, when wet 0.46; RMSE of moss when dry was

Table 7. Modeled ET_p and ET_a for different surfaces in a lysimeter (lys.) and for a situation with deep groundwater levels (gw. ind.) for the year 2013.

	ET_p (mm)	ET_a lys. (mm)	ET_a gw. ind. (mm)
Bare sand	400	295	258
Moss (*Campylopus int.*)	468	312	272
Moss (*Hypnum cup.*)	468	–	182
Grass	392	350	333
Grass, no dieback	429 (+9 %)	382 (+9 %)	362 (+9 %)
Heather	549	460	391
Heather, no dieback	610 (+11 %)	499 (+8 %)	420 (+7 %)

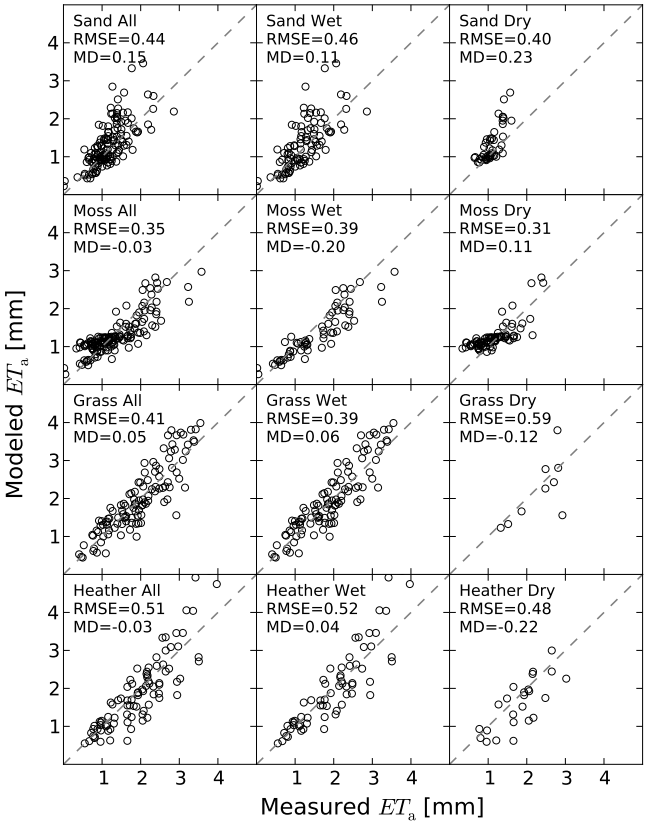

Figure 10. Measured vs. modeled ET_a of the lysimeters for all, wet ($ET_{a,mod} = ET_p$) and dry ($ET_{a,mod} \neq ET_p$) days. Dotted lines represent the 1 : 1 lines.

0.30, when wet 0.39), suggesting that our simplified model could describe the dominant processes and the simulation of vapor flow was not required for the temperate climate of our study area.

One would expect oasis effects to occur in the vicinity of the lysimeters, because freely draining lysimeters must saturate at the bottom of the lysimeter tank before water drains out. This enlarges the water availability inside the lysimeters compared to its groundwater-independent surroundings and occasionally leads to a situation in which the vegetation inside the lysimeters is still transpiring, while the vegetation outside the lysimeters becomes water-stressed and heats up. In such a situation, advection of sensible heat generated in the vicinity of the lysimeters could contribute to the available energy for lysimeter evapotranspiration. However, calculated ET_p was seldom smaller than measured lysimeter ET_a, indicating that oasis effects were absent. Furthermore, if oasis effects were prominent, systematic underestimation of modeled lysimeter ET_a would occur, since we ignored the possible contribution of heat advection. Note that it is very unlikely that oasis effects affected the back-calculated surface resistances (Table 5), since these were based on days after rain events for which we may assume ET_a to be equal to ET_p for both the lysimeters and their surroundings.

Neglecting feedbacks of drought on the transpiring leaf area and thereby the surface resistance (i.e., using a fixed r_s) of heather and dry grassland vegetation leads to an overestimation of cumulative ET_a of 7–9 % for years with relatively severe drought (Table 7). The delayed drought response of these vegetation types is therefore of importance to water balance studies, especially when, according to the expectations, summers become dryer as a result of a changing climate. Longer recordings of ET_a in heathland and grassland are required to understand and parameterize the drought response of these vegetation types in coupled plant physiological and hydrometeorological models.

To our knowledge, this paper describes for the first time the evaporation characteristics of a moss surface in a dune ecosystem in a temperate climate. The evaporation rate of the dense moss mat *Campylopus introflexus* is 5 % larger than the evaporation rate of bare sand. *Campylopus introflexus* forms dense moss mats and of the moss species investigated by Voortman et al. (2014), it has the largest water-holding capacity. Voortman et al. (2014) hypothesized that moss-covered soils could be more economical with water than bare soils, since the unsaturated hydraulic properties of moss layers reduce the magnitude of evaporation under relatively moist conditions. Our simulations of evaporation from the more open-structured *Hypnum cupressiforme* moss species (common in coastal dunes), which primarily differs in moisture content near saturation compared to *Campylopus introflexus* (0.20 instead of 0.61), confirms this hypothesis. The simulated evaporation rate for this species was 29 % lower than the evaporation rate of bare soil. From both our measurements and model simulations, xerophytic (drought-tolerant) mosses appear to be very economical with water; their evaporation rate is comparable with that of bare sand, or lower.

Campylopus introflexus is considered an invasive species in the Northern Hemisphere and was first discovered in Europe in 1941 (Klinck, 2010). Considering the large difference in yearly evaporation between *Hypnum cupressiforme* and *Campylopus introflexus* species (90 mm), the invasion of the *Campylopus introflexus* could have had negative impacts on water resources in specific areas which were previously dominated by more open-structured moss species with poorer wa-

ter retention characteristics. For sustainable management of groundwater resources in coastal and inland sand dunes, an accurate estimate of the groundwater recharge is required. For consultancy about the availability of water, moss species cannot be categorized in a singular plant functional type, since the modulating effect of the moss cover is species-specific. However, in terms of water retention characteristics, the species investigated by Voortman et al. (2014) are distinguished from each other by the water-holding capacity near saturation (θ_0, Appendix A), which is easily measured in a laboratory. Moss species could be categorized by this characteristic.

Mosses and lichens are common in early successional stages after colonizing and stabilizing drift sand or as understory vegetation in heathlands or grasslands. Vascular plants might benefit from the presence of certain moss species as more water may be conserved in the root zone. On the other hand, field observations show that moss- and lichen-rich vegetation can persist for many decades (Daniëls et al., 2008). Detailed measurements of understory evaporation in heathlands and grasslands are required to unravel the ecological interactions between mosses and vascular plants.

4 Conclusions

In this study, the net longwave radiation (R_{nl}) appeared to be one of the largest energy fluxes in dune vegetation. The poor performance of the calibrated FAO-56 approach for simulating R_{nl} for hourly time steps illustrates that this energy flux has attracted insufficient attention in evapotranspiration research. The novel approach presented in this study to simulate R_{nl} outperformed the calibrated FAO-56 approach and forms an accurate alternative for estimating R_{nl}.

A relatively simple hydrological model could be used to simulate evapotranspiration of dry dune vegetation with satisfactory results. Improvements in terms of climate robustness would be especially achieved if plant physiological processes were integrated in the hydrometeorological model. Without considering the effects of dry spells on the surface resistance (r_s) of grassland and heathland vegetation, ET_a would be overestimated with 9 and 7 % for years with relatively severe drought (drought events with a reoccurrence of once per 5 years).

Moss species are very economical with water. The evaporation of moss surfaces is comparable or even lower than bare sand. By promoting moss-dominated ecosystems in coastal and inland dunes, the evapotranspiration could be reduced considerably, to the benefit of the groundwater system. Differences in evaporation between moss species are large and should be considered in water balance studies.

Long-term measurements of ET_a in heathland and grassland are required to study feedbacks between climate and plant physiological processes in order to integrate the drought response of natural vegetation in coupled plant physiological and hydrometeorological models. To understand the ecological interaction between mosses and vascular plants, detailed measurements of understory evaporation in heathlands and grasslands are required.

Appendix A: Soil hydraulic properties for the simulation of unsaturated flow with Hydrus-1D

Unsaturated flow in Hydrus 1D is described by a modified form of Richards' equation:

$$\frac{\partial \theta}{\partial t} = \frac{\partial}{\partial z}\left(K\frac{\partial h}{\partial z} + K\right), \tag{A1}$$

where K is the unsaturated conductivity ($\mathrm{L\,T^{-1}}$), z is the vertical coordinate (L) and t is the time (T). The soil hydraulic properties were assumed to be described by the Mualum van Genuchten functions:

$$\theta(h) = \theta_\mathrm{r} + \frac{\theta_0 - \theta_\mathrm{r}}{[1 + |\alpha h|^n]^m} \tag{A2}$$

$$K(\theta) = K_0 S_\mathrm{e}^l \left[1 - \left(1 - S_\mathrm{e}^{1/m}\right)^m\right]^2 \tag{A3}$$

with

$$S_\mathrm{e}(h) = \frac{\theta(h) - \theta_\mathrm{r}}{\theta_0 - \theta_\mathrm{r}}, \tag{A4}$$

where θ is the volumetric water content ($\mathrm{L^3\,L^{-3}}$), h is the soil water pressure head (L), θ_0 is an empirical parameter matching measured and modeled θ ($\mathrm{L^3\,L^{-3}}$), θ_r is the residual water content ($\mathrm{L^3\,L^{-3}}$) and α ($\mathrm{L^{-1}}$) and n (–) are empirical shape parameters of the retention function. K_0 is an empirical parameter, matching measured and modeled K ($\mathrm{L\,T^{-1}}$), S_e is the effective saturation (–), l is the pore-connectivity parameter (–) and m ($= 1 - 1/n$) (–) is an empirical parameter. Drying retention data of two soil samples collected next to each lysimeter at 5 and 15 cm depth were used to fit a retention function with the RETC code (Van Genuchten et al., 1991). Hysteresis in the retention function was accounted for by assuming the retention curve parameter α for the wetting curve (α_wet) to be twice as large as α of the drying retention curve (α_dry) (Šimůnek et al., 1999). The unsaturated hydraulic conductivity parameters l and K_0 were estimated using the Rosetta database and pedotransfer functions, providing the fitted drying retention curve parameters as input (Schaap et al., 2001). Average parameter values per lysimeter are summarized in Table A1.

The hydraulic properties of the 15 cm long wick, guiding drainage water below the lysimeter into the tipping bucket, were taken from Knutson and Selker (1994) who analyzed the same brand and type of wick, i.e., Peperell 1/2 inch. The K_0 of the wick was adjusted to correct for the smaller cross-sectional area of the wick compared to the cross-sectional area of the lysimeter in the 1-D model simulation (Table A1).

The heterogeneous pore structure of the moss material was described by the functions of Durner (1994):

$$S_\mathrm{e} = w_1\left(1 + [\alpha_1 h]^{n_1}\right)^{-m_1} + w_2\left(1 + [\alpha_2 h]^{n_2}\right)^{-m_2} \tag{A5}$$

$$K(S_\mathrm{e}) = K_\mathrm{s}\frac{\left(w_1 S_{\mathrm{e}_1} + w_2 S_{\mathrm{e}_2}\right)^l \left(w_1\alpha_1\left[1 - \left(1 - S_{\mathrm{e}_1}^{1/m_1}\right)^{m_1}\right] + w_2\alpha_2\left[1 - \left(1 - S_{\mathrm{e}_2}^{1/m_2}\right)^{m_2}\right]\right)^2}{\left(w_1\alpha_1 + w_2\alpha_2\right)^2}, \tag{A6}$$

where w_1 and w_2 are weighting factors for two distinct pore systems of the moss layer, a capillary pore system (subscript 1) and a macropore system active near saturation ($h > -1$ cm, subscript 2), and K_s is the hydraulic conductivity at saturation. Average hydraulic parameters of the capillary pore system and the volumetric portion of the macropore system of the moss species *Campylopus introflexus* and *Hypnum cupressiforme* were taken from Voortman et al. (2014) (illustrated with dotted lines in Figs. A1 and A2). The α_2 parameter was fitted to the functions of Voortman et al. (2014) using $K_\mathrm{s} = 1000\,\mathrm{cm\,d^{-1}}$ and $n_2 = 2$ by minimizing the RMSE by generalized reduced gradient nonlinear optimization. Hydraulic parameter values are listed in Table A2.

Table A1. Hydraulic parameter values of lysimeter soils.

	θ_r (–)	θ_0 (–)	α_{dry} (cm^{-1})	α_{wet} (cm^{-1})	n (–)	K_0 ($cm\,h^{-1}$)	L (–)
Bare sand	0.01	0.367	0.023	0.046	2.945	1.042	−0.401
Moss	0.01	0.397	0.019	–	2.335	0.734	−0.173
Grass	0.01	0.401	0.025	0.050	2.071	1.119	−0.278
Heather	0.01	0.392	0.018	0.036	2.581	0.679	−0.186
Wick	0.00	0.630	0.098	0.196	3.610	2.180	0.500

Table A2. Hydraulic parameter values of the two moss species.

	θ_r (–)	θ_s (–)	α_1 (cm^{-1})	n (–)	K_s ($cm\,h^{-1}$)	l (–)	w_2 (–)	α_2 (cm^{-1})	n_2 (–)
Campylopus int.	0.060	0.936	0.080	2.25	41.67	−2.69	0.371	45.89	2.00
Hypnum cup.	0.010	0.971	0.013	2.17	41.67	−2.37	0.800	16.61	2.00

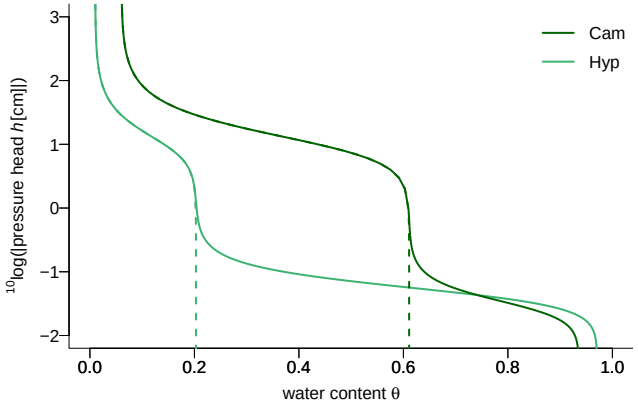

Figure A1. Water retention functions of two moss species: *Campylopus introflexus* and *Hypnum cupressiforme*. The dotted lines indicate the contribution of the capillary pore system, characterized by Voortman et al. (2014).

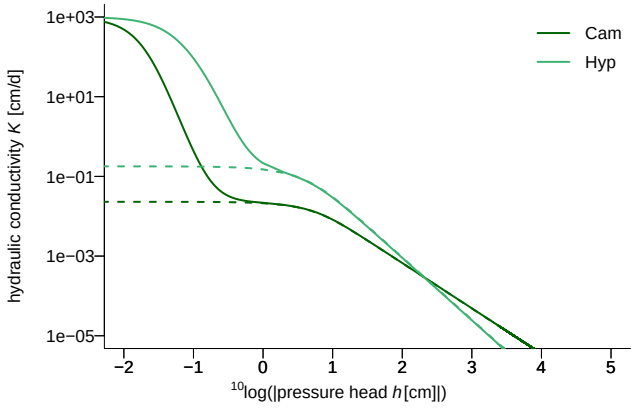

Figure A2. Hydraulic conductivity functions for two moss species: *Campylopus introflexus* and *Hypnum cupressiforme*. The dotted lines indicate the contribution of the capillary pore system, characterized by Voortman et al. (2014).

Appendix B: Feddes function used in the Hydrus 1-D model to simulate the closure of leaf stomata during water-stressed periods

The Feddes function (Feddes et al., 1978) describes the relative transpiration rate in relation to the soil water pressure head (Fig. B1) (being 0 if transpiration ceases and 1 if it equals potential rate). Near-positive pressure heads, root water uptake ceases due to oxygen stress (P0). At the dry end of the function, root water uptake ceases (P3). The moment at which transpiration becomes limited due to moisture stress is dependent on the potential transpiration rate. At a high potential transpiration rate (5 mm d^{-1} in the model simulation), leaf stomata start to close earlier (P2H) than under a low potential transpiration rate (P2L, 1 mm d^{-1} in the model simulation). Values for the parameters of Fig. B1 are listed in Table B1.

‘

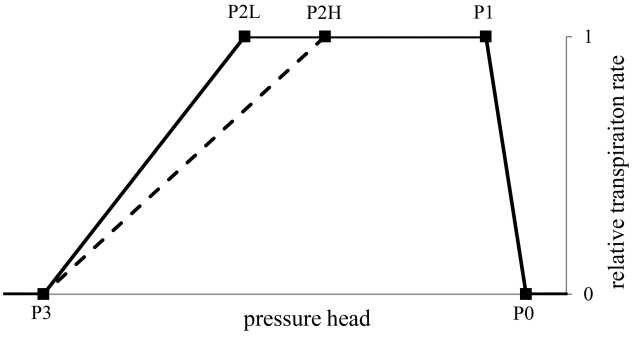

Figure B1. The relative transpiration rate as a function of soil water pressure head according to Feddes et al. (1978).

Table B1. Parameters of the water stress reduction function used in the Hydrus 1-D model.

P0 (cm)	P1 (cm)	P2H (cm)	P2L (cm)	P3 (cm)	r2H (mm h^{-1})	r2L (mm h^{-1})
−10	−25	−300	−1000	−8000	5	1

Acknowledgements. This study was carried out within the joint research programme of the Dutch Water Utility sector (http://www.kwrwater.nl/BTO), and the project Climate Adaptation for Rural Areas (CARE), which was funded by the Knowledge for Climate Program (http://knowledgeforclimate.climateresearchnetherlands.nl/climateadaptationforruralareas).
We thank the staff of Vitens for their permission to perform hydrometeorological measurements in one of their drinking water extraction sites.

Edited by: I. Neuweiler

References

Allen, R. G., Pruitt, W. O., and Jensen M. E.: Environmental requirements of lysimeters, in: Lysimeters for evapotranspiration and environmental measurements, edited by: Allen, R. G., Howell, T. A., Pruitt, W. O., Walter, I. A., and Jensen, M. E., American Society of Civil Engineers, New York, 170–181, 1991.

Allen, R. G., Pereira, L. S., Raes, D., and Smith, M.: Crop Evapotranspiration-Guidelines for Computing Crop Water Requirements, FAO irrigation and drainage paper 56, United Nations Food and Agriculture Orginization, Rome, 1998.

ASCE-EWRI: The ASCE Standardized Reference Evapotranspiration Equation, Environmental and Water Resources Institure of the American Society of Civil Engineers, Reston, Verginia, USA, 2005.

Bastiaanssen, W. G. M., Menenti, M., Feddes, R. A., and Holtslag, A. A. M.: A remote sensing Surface Energy Balance Algorithm for Land (SEBAL). 1. Formulation, J. Hydrol., 212–213, 198–212, doi:10.1016/S0022-1694(98)00253-4, 1998.

Blonquist Jr., J. M., Allen, R. G., and Bugbee, B.: An evaluation of the net radiation sub-model in the ASCE standardized reference evapotranspiration equation: implications for evapotranspiration prediction, Agr. Water Manage., 97, 1026–1038, doi:10.1016/j.agwat.2010.02.008, 2010.

Boulet, G., Braud, I., and Vauclin, M.: Study of the mechanisms of evaporation under arid conditions using a detailed model of the soil-atmosphere continuum. Application to the EFEDA I experiment, J. Hydrol., 193, 114–141, doi:10.1016/S0022-1694(96)03148-4, 1997.

Brunt, D.: Notes on radiation in the atmosphere. I, Q. J. Roy. Meteor. Soc., 58, 389–420, doi:10.1002/qj.49705824704, 1932.

Cameron, K. C., Smith, N. P., McLay, C. D. A., Fraser, P. M., McPherson, R. J., Harrison, D. F., and Harbottle, P.: Lysimeters without edge flow: an improved design and sampling procedure, Soil Sci. Soc. Am. J., 56, 1625–1628, doi:10.2136/sssaj1992.03615995005600050048x, 1992.

Campbell Scientific Inc.: Model HFP01SC Self-Calibrating Soil Heat Flux Plate, Logan, Utah, 24 pp., 2014.

Corwin, D. L.: Evaluation of a simple lysimeter-design modification to minimize sidewall flow, J. Contam. Hydrol., 42, 35–49, doi:10.1016/S0169-7722(99)00088-1, 2000.

Daniëls, F. J. A., Minarski, A., and Lepping, O.: Dominance pattern changes of a lichen-rich corynephorus grassland in the inland of the Netherlands, Annali di Botanica, VIII, 9–19, 2008.

Delpla, I., Jung, A. V., Baures, E., Clement, M., and Thomas, O.: Impacts of climate change on surface water quality in relation to drinking water production, Environ. Int., 35, 1225–1233, doi:10.1016/j.envint.2009.07.001, 2009.

Dolman, A. J.: Predicting evaporation from an oak forest, PhD thesis, University of Groningen, Netherlands, 91 pp., 1987.

Durner, W.: Hydraulic conductivity estimation for soils with heterogeneous pore structure, Water Resour. Res., 30, 211–223, doi:10.1029/93wr02676, 1994.

Feddes, R. A., Kowalik, P. J., and Zaradny, H.: Simulation of Field Water Use and Crop Yield, Pudoc, Wageningen, Netherlands, 1978.

Federer, C. A., Vörösmarty, C., and Fekete, B.: Intercomparison of methods for calculating potential evaporation in regional and global water balance models, Water Resour. Res., 32, 2315–2321, doi:10.1029/96wr00801, 1996.

Friedl, M. A.: Relationships among remotely sensed data, surface energy balance, and area-averaged fluxes over partially vegetated land surfaces, J. Appl. Meteorol., 35, 2091–2103, doi:10.1175/1520-0450(1996)035<2091:rarsds>2.0.co;2, 1996.

Fuchs, M. and Tanner, C. B.: Surface temperature measurements of bare soils, J. Appl. Meteorol., 7, 303–305, doi:10.1175/1520-0450(1968)007<0303:stmobs>2.0.co;2, 1968.

Gavilán, P., Estévez, J., and Berengena, J.: Comparison of standardized reference evapotranspiration equations in Southern Spain, J. Irrig. Drain. E.-ASCE, 134, 1–12, 2008.

Gavriliev, R. I.: Therma properties of soils and surface covers, in: Thermal Analysis, Construction, and Monitoring Methods for Frozen Ground, edited by: Esch, D. C., American Society of Civil Engineers, Restion, Verginia, USA, 277–295, 2004.

Gubler, S., Gruber, S., and Purves, R. S.: Uncertainties of parameterized surface downward clear-sky shortwave and all-sky longwave radiation., Atmos. Chem. Phys., 12, 5077–5098, doi:10.5194/acp-12-5077-2012, 2012.

Hollinger, D. Y., Ollingerw, S. V., Richardsonw, A. D., Meyersz, T. P., Dail, D. B., Martinw, M. E., Scott, N. A., Arkebauerk, T. J., Baldocchi, D. D., Clark, K. L., Curtis, P. S., Davis, K. J., Desai, A. R., Dragonikk, D., Goulden, M. L., Gu, L., Katulzzz, G. G., Pallardy, S. G., Pawu, K. T., Schmid, H. P., Stoy, P. C., Suyker, A. E., and Verma, S. B.: Albedo estimates for land surface models and support for a new paradigm based on foliage nitrogen concentration, Glob. Change Biol., 16, 696–710, 2010.

Irmak, S., Howell, T. A., Allen, R. G., Payero, J. O., and Martin, D. L.: Standardized ASCE Penman–Monteith: impact of sum-of-hourly vs. 24 h timestep computations at reference weather station sites, T. ASABE, 48, 1063–1077, 2005.

Irmak, S., Mutiibwa, D., and Payero, J. O.: Net radiation dynamics: performance of 20 daily net radiation models as related to model structure and intricacy in two climates, T. ASABE, 53, 1059–1076, 2010.

Jones, H. G.: Application of Thermal Imaging and Infrared Sensing in Plant Physiology and Ecophysiology, Adv. Bot. Res., 41, 107–163, doi:10.1016/S0065-2296(04)41003-9 2004.

Kay, A. L., Bell, V. A., Blyth, E. M., Crooks, S. M., Davies, H. N., and Reynard, N. S.: A hydrological perspective on evaporation: historical trends and future projections in Britain, Journal of Water and Climate Change, 4, 193–208, doi:10.2166/wcc.2013.014, 2013.

Klinck, J.: NOBANIS Invasive Alien Species Fact Sheet Campylopus introflexus, from: Online Database of the North European and Baltic Network on Invasive Alien Species – NOBANIS,

available at: www.nobanis.org, last access: 9 February 2015, 2010.

Knutson, J. H. and Selker, J. S.: Unsaturated hydraulic conductivities of fiberglass wicks and designing capillary wick pore-water samplers, Soil Sci. Soc. Am. J., 58, 721–729, 1994.

Kustas, W. P. and Daughtry, C. S. T.: Estimation of the soil heat flux/net radiation ratio from spectral data, Agr. Forest Meteorol., 49, 205–223, doi:10.1016/0168-1923(90)90033-3, 1990.

Kustas, W. P., Zhan, X., and Schmugge, T. J.: Combining optical and microwave remote sensing for mapping energy fluxes in a semiarid watershed, Remote Sens. Environ., 64, 116–131, doi:10.1016/S0034-4257(97)00176-4, 1998.

Ladekarl, U. L., Rasmussen, K. R., Christensen, S., Jensen, K. H., and Hansen, B.: Groundwater recharge and evapotranspiration for two natural ecosystems covered with oak and heather, J. Hydrol., 300, 76–99, doi:10.1016/j.jhydrol.2004.05.003, 2005.

Liakatas, A., Clark, J. A., and Monteith, J. L.: Measurements of the heat balance under plastic mulches. Part I. Radiation balance and soil heat flux, Agr. Forest Meteorol., 36, 227–239, doi:10.1016/0168-1923(86)90037-7, 1986.

Linacre, E. T.: Net radiation to various surfaces, J. Appl. Ecol., 6, 61–75, doi:10.2307/2401301, 1969.

Liu, S., Graham, W. D., and Jacobs, J. M.: Daily potential evapotranspiration and diurnal climate forcings: influence on the numerical modelling of soil water dynamics and evapotranspiration, J. Hydrol., 309, 39–52, 2005.

López-Urrea, R., Olalla, F. M. D. S., Fabeiro, C., and Moratalla, A.: An evaluation of two hourly reference evapotranspiration equations for semiarid conditions, Agr. Water Manage., 86, 277–282, 2006.

Makkink, G. G.: Testing the Penman formula by means of lysimeters, J. Inst. Wat. Engrs., 11, 277–288, 1957.

Matsui, H.: Comparison of net longwave radiation equation in Penman-type evapotranspiration equation, Transactions of The Japanese Society of Irrigation, Drain. Rural Eng., 78, 531–536, doi:10.11408/jsidre.78.531, 2010.

Miranda, A. C., Jarvis, P. G., and Grace, J.: Transpiration and evaporation from heather Moorland, Bound.-Lay. Meteorol., 28, 227–243, doi:10.1007/bf00121306, 1984.

Monteith, J. L. and Unsworth, M. H.: Principles of Envoronmental Physics, Edward Arnold, London, 1990.

Moors, E. J.: Water Use of Ferest in the Netherlands, PhD thesis, Vrije Universiteit Amsterdam, Amsterdam, the Netherlands, 2012.

Nozue, K. and Maloof, J. N.: Diurnal regulation of plant growth, Plant Cell Environ., 29, 396–408, doi:10.1111/j.1365-3040.2005.01489.x, 2006.

Oke, T. R.: Boundary Layer Climates, Methuen & Co Ltd, London, 372 pp., 1978.

Penman, H. L.: Natural evaporation from open water, bare soil and grass, P. Roy. Soc. Lond. A-Mat., 193, 120–145, doi:10.1098/rspa.1948.0037, 1948.

Perera, K. C., Western, A. W., Nawarathna, B., and George, B.: Comparison of hourly and daily reference crop evapotranspiration equations across seasons and climate zones in Australia, Agr. Water Manage., 148, 84–96, doi:10.1016/j.agwat.2014.09.016, 2015.

Price, J. S., Edwards, T. W. D., Yi, Y., and Whittington, P. N.: Physical and isotopic characterization of evaporation from Sphagnum moss, J. Hydrol., 369, 175–182, 2009.

Proctor, M. C. F., Oliver, M. J., Wood, A. J., Alpert, P., Stark, L. R., Cleavitt, N. L., and Mishler, B. D.: Desiccation-tolerance in bryophytes: A review, Bryologist, 110, 595–621, doi:10.1639/0007-2745(2007)110[595:DIBAR]2.0.CO;2, 2007.

Qiu, G. Y., Yano, T., and Momii, K.: An improved methodology to measure evaporation from bare soil based on comparison of surface temperature with a dry soil surface, J. Hydrol., 210, 93–105, 1998.

Saffigna, P. G., Kenney, D. R., and Tanner, C. B.: Lysimeter and field measurements of chloride and bromide leaching in an uncultivated loamy sand, Soil Sci. Soc. Am. J., 41, 478–482, 1977.

Saito, H. and Šimůnek, J.: Effects of meteorological models on the solution of the surface energy balance and soil temperature variations in bare soils, J. Hydrol., 373, 545–561, doi:10.1016/j.jhydrol.2009.05.019, 2009.

Schaap, M. G., Leij, F. J., and Van Genuchten, M. T.: Rosetta: a computer program for estimating soil hydraulic parameters with hierarchical pedotransfer functions, J. Hydrol., 251, 163–176, doi:10.1016/S0022-1694(01)00466-8, 2001.

Schelde, K., Thomsen, A., Heidmann, T., Schjønning, P., and Jansson, P. E.: Diurnal fluctuations of water and heat flows in a bare soil, Water Resour. Res., 34, 2919–2929, doi:10.1029/98wr02225, 1998.

Shuttleworth, W. J.: Putting the "vap" into evaporation, Hydrol. Earth Syst. Sci., 11, 210–244, doi:10.5194/hess-11-210-2007, 2007.

Šimůnek, J., Kodešová, R., Gribb, M. M., and Van Genuchten, M. T.: Estimating hysteresis in the soil water retention function from cone permeameter experiments, Water Resour. Res., 35, 1329–1345, doi:10.1029/1998wr900110, 1999.

Šimůnek, J., Šejna, M., Saito, H., Sakai, M., and Van Genuchten, M. T.: The Hydrus-1D Software Package for Simulating the movement of water, heat, and multiple solutes in variably saturated media, version 4.0, HYDRUS Softwater Series 3, Department of Environmental Sciences, University of California Riverside, Riverside, 2008.

Su, Z.: The Surface Energy Balance System (SEBS) for estimation of turbulent heat fluxes, Hydrol. Earth Syst. Sci., 6, 85–100, doi:10.5194/hess-6-85-2002, 2002.

Temesgen, B., Eching, S., and Frame, K.: Comparing net radiation estimation methods: CIMIS versus Penman–Monteith, J. Irrig. Drain. E.-ASCE, 133, 265–271, doi:10.1061/(ASCE)0733-9437(2007)133:3(265), 2007.

Till, A. R. and McCabe, T. P.: Sulfur leaching and lysimeter characterization, Soil Sci., 121, 44–47, 1976.

Van Bavel, C. H. M. and Hillel, D. I.: Calculating potential and actual evaporation from a bare soil surface by simulation of concurrent flow of water and heat, Agr. Meteorol., 17, 453–476, doi:10.1016/0002-1571(76)90022-4, 1976.

Van de Griend, A. A. and Owe, M.: Bare soil surface resistance to evaporation by vapor diffusion under semiarid conditions, Water Resour. Res., 30, 181–188, doi:10.1029/93wr02747, 1994.

Van Genuchten, M. T.: A closed-form equation for predicting the hydraulic conductivity of unsaturated soils, Soil Sci. Soc. Am. J., 44, 892–898, doi:10.2136/sssaj1980.03615995004400050002x, 1980.

Van Genuchten, M. T., Leij, F. J., and Yates, S. R.: The RETC Code for Quantifying the Hydraulic Functions of Unsaturated Soils, Version 1.0, Salinity Laboratory, USDA, ARS, Riverside, California, 1991.

van Vliet, M. T. H. and Zwolsman, J. J. G.: Impact of summer droughts on the water quality of the Meuse river, J. Hydrol., 353, 1–17, doi:10.1016/j.jhydrol.2008.01.001, 2008.

Van Wijk, W. R. and Scholte Ubing, D. W.: Radiation, in: Physics of Plant Environment, edited by: Van Wijk, W. R., North-Holland Publishing, Amsterdam, the Netherlands, 62–101, 1963.

Voortman, B. R., Bartholomeus, R. P., Van Bodegom, P. M., Gooren, H., Van Der Zee, S. E. A. T. M., and Witte, J. P. M.: Unsaturated hydraulic properties of xerophilous mosses: towards implementation of moss covered soils in hydrological models, Hydrol. Process., 28, 6251–6264, doi:10.1002/hyp.10111, 2014.

Wallace, J. S., Lloyd, C. R., Roberts, J., and Shuttleworth, W. J.: A comparison of methods for estimating aerodynamic resistance of heather (*calluna vulgaris* (L.) hull) in the field, Agr. Forest Meteorol., 32, 289–305, doi:10.1016/0168-1923(84)90055-8, 1984.

Wouters, D. S., Keppens, H., and Impens, I.: Factors determining the longwave radiation exchange over natural surfaces, Arch. Meteor. Geophy. B., 28, 63–71, doi:10.1007/bf02243835, 1980.

Yang, F., Mitchell, K., Hou, Y.-T., Dai, Y., Zeng, X., Wang, Z., and Liang, X.-Z.: Dependence of land surface albedo on solar zenith angle: observations and model parameterization, J. Appl. Meteorol. Clim., 47, 2963–2982, doi:10.1175/2008jamc1843.1, 2008.

Yin, Y., Wu, S., Zheng, D., and Yang, Q.: Radiation calibration of FAO56 Penman–Monteith model to estimate reference crop evapotranspiration in China, Agr. Water Manage., 95, 77–84, doi:10.1016/j.agwat.2007.09.002, 2008.

Zhang, Y.-F., Wang, X.-P., Hu, R., Pan, Y.-X., and Zhang, H.: Variation of albedo to soil moisture for sand dunes and biological soil crusts in arid desert ecosystems, Environ. Earth Sci., 71, 1281–1288, doi:10.1007/s12665-013-2532-7, 2013.

Zhou, M. C., Ishidaira, H., Hapuarachchi, H. P., Magome, J., Kiem, A. S., and Takeuchi, K.: Estimating potential evapotranspiration using Shuttleworth–Wallace model and NOAA-AVHRR NDVI data to feed a distributed hydrological model over the Mekong River basin, J. Hydrol., 327, 151–173, 2006.

Zwolsman, J. J. G. and van Bokhoven, A. J.: Impact of summer droughts on water quality of the Rhine River – a preview of climate change?, Water Sci. Technol., 56, 45–55, 2007.